Influence of Pyrene-Labeling on Fluid Lipid Membranes

Jarmila Repáková

Laboratory of Physics and Helsinki Institute of Physics, Helsinki University of Technology, Helsinki, Finland

Juha M. Holopainen

Department of Ophthalmology and Helsinki Biophysics and Biomembrane Group, Institute of Biomedicine, University of Helsinki, Helsinki, Finland

Mikko Karttunen

Department of Applied Mathematics, University of Western Ontario, London (ON), Canada

Ilpo Vattulainen*

Institute of Physics, Tampere University of Technology, Tampere, Finland; Laboratory of Physics and Helsinki Institute of Physics, Helsinki University of Technology, Helsinki, Finland; and Memphys-Center for Biomembrane Physics, Physics Department, University of Southern Denmark, Odense, Denmark

Received: March 1, 2006; In Final Form: June 1, 2006

We elucidate the influence of pyrene-labeled phospholipids on the structural properties of a fluid dipalmitoylphosphatidylcholine lipid membrane. To this end, we employ extensive atomic-scale molecular dynamics simulations with varying concentrations of pyrene-linked lipids. We find pyrene labeling to perturb the membrane structure significantly in the vicinity of the probe, the correlation length in the bilayer plane being about 1.0−1.5 nm. The local perturbations lead to enhanced ordering and packing of lipid acyl chains located in the vicinity of the probe. Surprisingly, this holds true not only for lipids that reside in the same leaflet as the pyrene-labeled probe but also for lipids in the opposite monolayer. The latter is due to substantial interdigitation of the pyrene moiety into the opposite leaflet, suggesting that occasional excimer formation may take place for probes in different leaflets. As a related issue, we also discuss the location and conformational orientation of the pyrene moieties. In particular, the orientational distribution of pyrene turns out to be more broad and diverse than the distribution of the corresponding acyl tails of nonlabeled lipids.

I. Introduction

Cellular membranes[1−3] surround cells as well as most cell compartments protecting their interior. In all biomembranes, the key component is a lipid bilayer comprised of two opposed leaflets in which various proteins and glycan-containing membrane anchors are embedded. These supramolecular systems serve as selective barriers, regulating the transport of a wide range of materials and containing the sites of action of many biologically active molecules such as proteins, hormones, and drugs.

Our understanding of membrane structure and its role in a variety of cellular processes is partially based on fluorescence spectroscopic measurements using fluorescent markers such as diphenylhexatriene and pyrene. The introduction of fluorescent probes into the membrane provides indirect but highly useful insight into membrane properties.[4−6] However, this gain is complemented by various potentially serious problems. First, it is evident that insertion of a probe into the membrane induces some structural perturbations, thus affecting the structure as well as dynamics of the native systems that one would like to characterize (see refs 7 and 8 and references therein). That renders the interpretation of experimental data rather difficult. Second, the use of fluorescent probes is associated with the uncertainty about their preferential locations and orientations in a membrane, as the interpretation of observed data from fluorescence experiments depends on where and how the probes are located within a membrane.

To avoid the above problems, one often employs fluorescent lipid analogues that mimic their natural counterparts as well as possible. Usually a fluorescent probe such as pyrene is linked to an acyl chain, thus replacing one of the lipid fatty acid chains. Pyrene, a hydrophobic dye shown in Figure 1 (attached to the *sn*-2 position), is particularly useful because its most characteristic features are the long lifetime (on the order of tens of nanoseconds) of the excited state and the formation of excimers (excited-state dimers).[4,5] These photophysical attributes are widely used in studies of numerous biophysical phenomena such as lateral arrangement and fluidity of membranes and membrane fusion and lipid trafficking in living cells.[5,9−12] Pyrene-derivated lipids are also commonly employed for detecting lipid domain formation and studies of lipid−protein interactions.[5,13,14]

The site of linkage of the pyrene fluorophore determines its intramolecular localization.[15] This implies that the location and orientation of the lipid-linked fluorophore within a bilayer is usually more sharply defined than in the case of a free probe. Also, the conformational arrangement of the bilayer system is expected to be sterically less perturbed when the probe is an integral part of a system component.[5] However, the main

* To whom correspondence should be addressed. E-mail: ilpo.vattulainen@csc.fi.

10.1021/jp061300r CCC: $33.50
Published on Web 07/15/2006

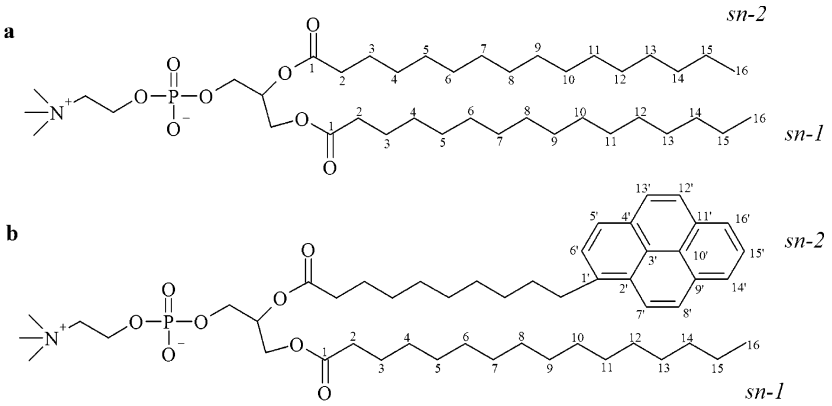

Figure 1. Structures of (a) DPPC and (b) PyrPC dye molecules used in this study.

disadvantage of pyrene-labeled lipid derivatives is the relatively large size of its fluorophore. One is tempted to assume that the bulky pyrene group attached to a lipid hydrocarbon chain may considerably affect the properties of the labeled molecule compared to native lipids as well as molecules that are in the vicinity of the probe. It is clear that a thorough evaluation of the detailed structure of these probes and their effects on the surroundings is necessary to correctly interpret and understand the data obtained through experiments.

Atomistic molecular dynamics (MD) simulations provide a unique tool to gain insight into macromolecular systems on atomistic and molecular scales. Computational studies can provide a great deal of insight into the molecular structure and dynamics of lipid membrane models.[16−18] Insight obtained through simulations can assist and complement the interpretation of experimental data. Most importantly, atomic-scale simulations provide detailed information about properties not accessible through experiments.

Recently, two computational studies of fluorescent probes in lipid bilayers have appeared in the literature. Our previous studies dealt with the properties of free diphenylhexatriene probes inside a dipalmitoylphosphatidylcholine (DPPC) bilayer, and their influence on bilayer structure and dynamics.[7,8] MD simulations, NMR, and differential scanning calorimetry experiments showed that these nonpolar probes prefer to reside in the hydrophobic region of the bilayer, where they give rise to major local perturbations such as enhanced acyl chain ordering and reduced lateral diffusion of lipids. The work by Hoff et al.[19] combined ^{2}H NMR measurements and MD simulations for the location and orientation of free pyrene probes inside a palmitoyloleoylphosphatidylcholine (POPC) bilayer. The simulation data revealed that pyrene prefers to reside in the ordered acyl chain region near lipid headgroups and orient itself parallel to the membrane normal.

In the present work, we study the properties of another commonly used fluorescent probe, the pyrene-labeled phospholipid analogue. We employ MD simulations to focus on the influence of pyrene-labeling on membrane structure. To our knowledge, this problem has not been addressed in molecular detail before. Our results show that pyrene-labeling gives rise to major local perturbations in the vicinity of the probe, but there are no signs of long-range effects. The pyrene-labeled lipid itself is highly ordered, and the orientational distribution of the pyrene moiety is more broad and diverse compared with that of the corresponding acyl tails of nonlabeled lipids. Consequently, the pyrene interdigitates to the opposed leaflet and perturbs lipids in that monolayer as well. Implications of these findings for experimental studies are discussed.

II. Model and Simulation Details

To evaluate the effects of fluorescent phospholipid analogues on the model membrane, we considered three systems with a different number of 1-palmitoyl-2-(1-pyrenedecanoyl)-*sn*-glycero-3-phosphocholine (PyrPC) molecules embedded in a DPPC bilayer in the biologically relevant fluid phase (see Figure 1). PyrPC concentrations of 0.8 mol % (1:127, the abbreviation here standing for the PyrPC/DPPC molar ratio), 3.2 mol % (4:124), and 4.9 mol % (6:122) were chosen to gauge the influence of PyrPC on membrane properties for a varying probe concentration and to observe possible clustering of pyrene moieties. In the case of the two higher concentrations of pyrene-linked lipids, an equal number of labeled molecules were introduced into both leaflets. For comparison, a MD simulation of a pure DPPC bilayer (0:128) was also carried out.

As an initial configuration, we used a fully hydrated, equilibrated lipid bilayer consisting of 128 DPPC molecules and 3655 water molecules obtained from our previous simulations.[8] A number of *sn*-2 acyl chains corresponding to the chosen concentration were randomly selected and replaced by pyrene. The systems with PyrPC molecules were then energy minimized using steepest descent to remove undesired contacts. The simulation box is oriented such that the bilayer lies in the *xy* plane and its *z*-axis is parallel to the lipid bilayer normal.

We used a united-atom description for CH, CH_2, and CH_3 groups in lipid and probe structures. The parameters for bonded and nonbonded interactions were taken from a study of a pure DPPC bilayer[20] available at http://moose.bio.ucalgary.ca/files/lipid.itp. The parameter set for PyrPC was taken from a similar combination of atom types in the DPPC model.[20] The partial charge distribution for atoms in a DPPC molecule has been described elsewhere[21] and can be found at http://moose.bio.ucalgary.ca/files/dppc.itp. For the pyrene moiety of PyrPC, we used no partial charges at all, as this part of the molecule is located in the hydrophobic region of a lipid bilayer. This choice was also supported by our ab initio quantum mechanical calculations of partial charges using the computing protocol explained in ref 21. Our calculations revealed that the partial charges on the pyrene moiety deviate only slightly from zero values. For water, we used the single-point charge model[22] with constraints (see below).

As for calculations of nonbonded interactions, we employed a cutoff at 1.0 nm for van der Waals as well as Lennard−Jones interactions. Long-range electrostatic interactions beyond the cutoff were determined every 10 time steps by the particle-mesh Ewald technique, which has performed well in recent membrane simulations.[23,24]

All MD simulations were carried out using the GROMACS simulation package (version 3.1.4)[25] under the conditions of constant pressure, constant temperature, and constant particle number (*NpT* ensemble). The temperature and the pressure of the system were controlled by the Berendsen algorithm[26] using time constants set to 0.1 ps and 1.0 ps, respectively. The semi-isotropic barostat used in the present work allows the height of the simulation box (in this case the *z* component) to change independently of the cross-sectional area of the system in the *xy* plane. All bond lengths were constrained using the LINCS algorithm.[27] The time step employed in the simulations was chosen to be 2.0 fs, and the instantaneous structures were saved every 10 ps. The MD simulations were carried out over a time scale of about 140 ns each. Periodic boundary conditions were applied in all three dimensions. The temperatures of DPPC, PyrPC, and water molecules were set separately to 325 K, which is above the main-phase transition temperature ($T_M \approx 315$ K) between the gel and liquid crystalline phases of a pure DPPC bilayer.[28]

To improve statistics of the data, the results have been averaged over the three PyrPC concentrations (unless mentioned otherwise), because the results of the 1:127, 4:124, and 6:122 systems were found to be largely identical. Doing this is of course based on the assumption that the results of PyrPC and PyrPC-induced perturbations do not significantly depend on the probe concentration. This assumption is in part supported by the experimental results of Martins and Melo,[9] who found that, within experimental error, the lateral diffusion coefficients of PyrPC in DMPC bilayers do not depend on the probe−phospholipid ratio. We will come back to this issue later in this article.

Snapshots of the simulated systems are shown in Figure 2.

III. Results

A. Area per Lipid and Equilibration. The central quantity in lipid bilayer systems describing molecular packing is the average area per molecule, $\langle A \rangle$, in the plane of the bilayer. It is commonly measured through experiments and serves as a good measure for assessing the validity of the model system. Besides that, $\langle A \rangle$ affects a variety of membrane properties such as lipid acyl chain ordering and lateral diffusion. Because of bilayer undulations and some approximations involved in the analysis, an accurate determination of this commonly measured quantity is not straightforward, however. Depending on the method used, experimental estimates for the area per DPPC in the fluid phase are scattered within a range from 0.56 nm^2 to 0.71 nm^2.[29] A more accurate estimate has been given by Nagle and Tristram-Nagle,[29] who have reanalyzed previous data and corrected this value to 0.64 nm^2.

In this work, the area per lipid was calculated by dividing the instantaneous area of the bilayer in the *xy* plane by the number of molecules in a monolayer (64). The profiles $A(t)$ for different concentrations of labeled lipids are shown in Figure 3. Based on the temporal fluctuations of the area per lipid, we concluded that equilibrium was attained within 10 ns of the simulations. Consequently, we discarded the first 10 ns of the trajectory and used the remaining part for further analysis.

Average values for $\langle A \rangle$ are given in Figure 3. Our result for the pure DPPC bilayer falls within the range of experimentally determined values. As for the influence of PyrPC, the average values for the area per molecule at higher PyrPC concentrations do not show significant changes with respect to a pure DPPC system.

Comparison to experiments is somewhat problematic because to our knowledge there are no data for the influence of PyrPC on the packing or the area per lipid in bilayer systems. For Langmuir monolayers, Somerharju et al.[30] observed that the average area per PyrPC was slightly larger than the average area in a DPPC bilayer. For a surface pressure of 30 dyn/cm, for example, they found the area per lipid increased from about 0.62 nm^2 for a pure DPPC bilayer to about 0.64 nm^2 in a bilayer of PyrPCs. However, it is not obvious that the comparison of

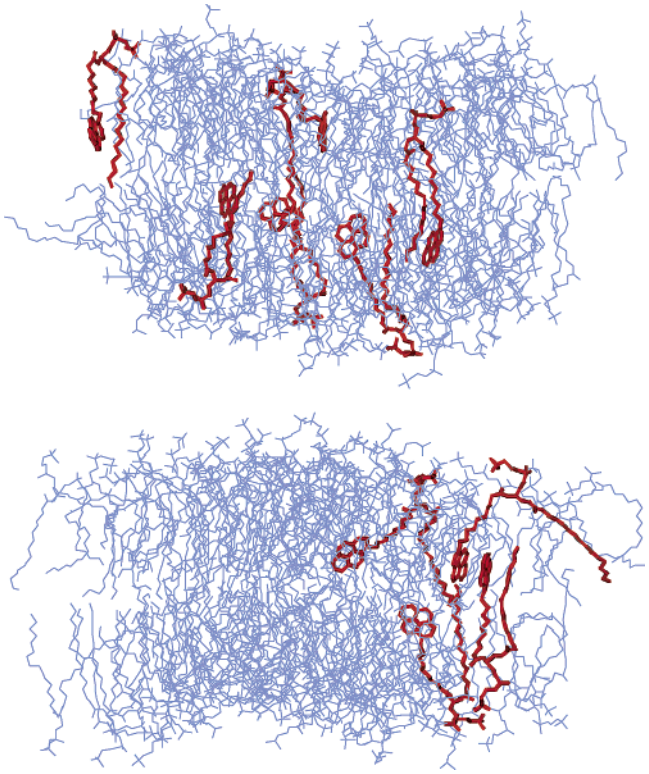

Figure 2. Snapshots of simulated bilayers in two cases. (a; upper) Bilayer configuration at 4.9 mol % of PyrPC showing an example of substantial penetration (interdigitation) to the opposing leaflet. (b; lower) Membrane system at 3.2 mol % of PyrPCs demonstrating excimer formation between pyrene moieties of PyrPCs in different leaflets; see the two molecules on the right-hand side. There is reason to stress, however, that interleaflet excimer formation seems to be a rare event. Water has been omitted to clarify the presentation.

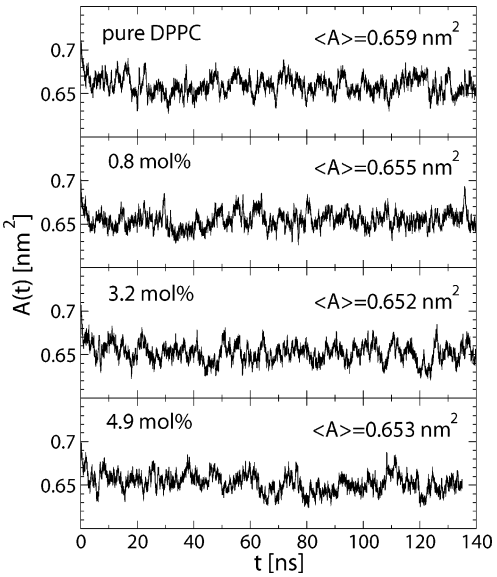

Figure 3. Time evolution of the area per lipid, $A(t)$, for different concentrations of PyrPC in a bilayer. For comparison, the average values after equilibration are also given. Error bars are about ±0.005 nm^2.

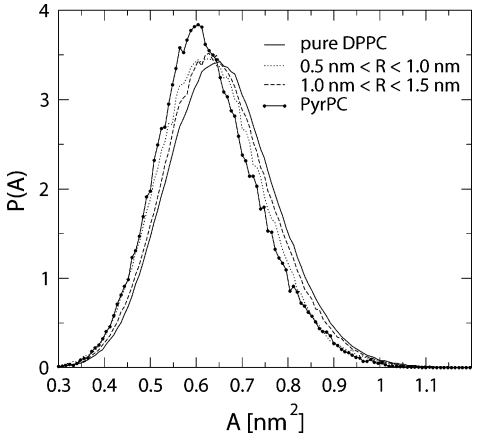

Figure 4. Probability distribution of the area per lipid $P(A)$ obtained by the Voronoi analysis. The results for DPPC molecules are shown as a function of the 3D distance R from the CM of DPPC to the CM of the nearest pyrene moiety. The results have been averaged over three systems.

our MD data for lipid bilayers with experimental data for Langmuir monolayers is meaningful. First, the Langmuir monolayer studies were conducted for a one-component system comprised of PyrPC lipids only, and the results were compared to a neat DPPC monolayer system. Clearly this setup differs substantially from ours. Second, recent studies have shown that lipid packing and the ordering of hydrocarbon chains in Langmuir films is clearly different from the behavior in lipid membranes.[31] Hence, it seems evident that there is no experimental data to which our simulation results could be directly compared.

For free pyrene, some remarks can be made, however. Hoff et al.[19] found through MD simulations at 300 K that the average area per lipid in a POPC membrane containing free pyrene molecules at a molar concentration of 4 mol % was about 0.57 nm^2. In a pure POPC bilayer, other MD studies have yielded a value of 0.655 nm^2 at 300 K and about 0.65 nm^2 at 310 K.[32] These studies hence propose that free pyrene gives rise to a decrease in the area per lipid in bilayers comprised of monounsaturated phospholipids. Recent MD studies for the effect of diphenylhexatriene in a DPPC bilayer are in line with this trend, as they also show a minor reduction in the average area per lipid.[8]

B. Distribution of Area around PyrPC. An alternative method for the calculation of the area per lipid is the Voronoi tessellation in two dimensions.[23] One advantage of this method is that it allows one to calculate the area for different types of lipid molecules in a system. In this technique, the center of mass (CM) positions of the molecules are first projected onto the xy plane separately for the two leaflets. The Voronoi tessellation then yields the area that is closer to a given molecule than to any other one. In this manner, we determined the area occupied by each individual lipid molecule for every frame and obtained the probability distribution of the area per molecule, $P(A)$, see Figure 4.

The results for $P(A)$ and the corresponding average values for the area per lipid are summarized in Figure 4 and Table 1, respectively. As is evident from Figure 4, the pyrene-labeled molecules occupy slightly less surface area compared with their unlabeled counterparts. Figure 4 further shows the influence of probe molecules on the packing of lipids surrounding PyrPC. In the vicinity of the pyrenyl group, the distribution of the area per DPPC is shifted toward lower values. This implies that the phospholipid molecules around the probe are more tightly packed. The condensing effect is of rather short range, though, being notable up to about 1.5 nm from the pyrenyl group. The short-range condensing effect and the small concentrations of PyrPC used here further explain why the average area per lipid across the whole system changes so little, see Figure 3.

TABLE 1: Average Values for the Area Per Molecule in Units of nm^2 Obtained from the Voronoi Analysis

molecule	conditions	$\langle A \rangle$
DPPC	all (pure DPPC)	0.659 ± 0.004
DPPC	$R > 1.5$ nm	0.657 ± 0.004
	1.0 nm $< R <$ 1.5 nm	0.650 ± 0.011
	0.5 nm $< R <$ 1.0 nm	0.636 ± 0.020
PyrPC	all	0.627 ± 0.035

C. Ordering of Acyl Chains. As the pyrene part of the probe molecule remains buried in the hydrophobic region of the lipid bilayer (see below), the most pronounced perturbations due to pyrene are expected in the properties of hydrocarbon chains. To quantify that region of the membrane, one of the most accurately determined properties of lipid membranes, available from NMR studies, is the deuterium order parameter $|S_{CD}|$. It provides information about lipid chain ordering with respect to the membrane normal and can be directly compared with results from simulations.

In simulations, the order parameter S_{CD} is evaluated through the order parameter tensor

$$S_{\alpha\beta} = \frac{1}{2}\langle 3 \cos \theta_\alpha \cos \theta_\beta - \delta_{\alpha\beta} \rangle$$

in which θ_α is the angle between the αth molecular axis and the bilayer normal. Due to molecular symmetry, the order parameter S_{CD} can be obtained through $S_{CD} = -S_{zz}/2$. To allow direct comparison with experimental data, we present the results from simulations in terms of $|S_{CD}|$. In addition to the order parameter profiles calculated for pure DPPC, the same characteristics were evaluated for labeled membranes as a function of the 3D distance from the CM of an acyl chain to the CM of the closest pyrene, R_{acyl}.

The order parameter profiles, $|S_{CD}|$, are shown in Figure 5. Our results for a pure DPPC system are consistent with experimental data.[33] As for the influence of the pyrene group on the ordering of acyl chains, we first readily observe a significant difference between the average ordering of DPPC and PyrPC molecules: the *sn*-1 acyl chains of PyrPC are substantially more ordered than the chains of unlabeled phospholipids. This is in line with the results in Table 1, indicating that PyrPCs are more strongly ordered and more tightly packed than native DPPCs. What comes to the ordering of DPPCs close to the probe, Figure 5 shows that PyrPC enhances the ordering of neighboring DPPC acyl chains in the same monolayer. These observations are also consistent with the decreased area per DPPC close to the pyrene, see Table 1. The most pronounced modifications in S_{CD} are observed for carbons in the middle of the acyl chains, where the pyrene group is preferentially located (see the next section and Figure 6). Nevertheless, the ordering effect due to pyrene is rather local and extends up to about two molecular diameters. Beyond this distance, the effect of pyrene is small, though a slight decrease in order parameter can be observed. This decrease is reflected for instance in the slightly decreased main phase transition temperature for DPPC/PyrPC mixtures revealed by differential scanning calorimetry.[34]

As for the *sn*-2 order parameter of PyrPC, the situation is more subtle because the ordering of carbons 2−10 is influenced by the orientational distribution of pyrene attached to the *sn*-2 chain. That is, the diverse orientations of pyrene discussed in

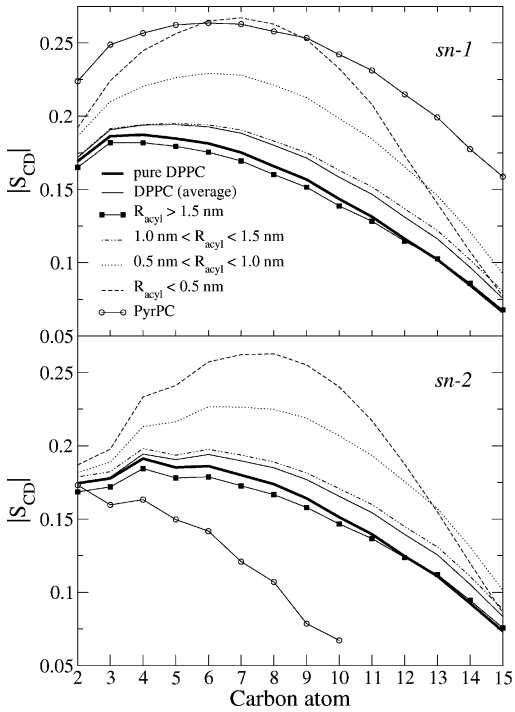

Figure 5. Order parameter $|S_{CD}|$ profiles for the *sn*-1 and *sn*-2 acyl chains of lipid molecules. Here, R_{acyl} is the 3D distance between the CM of a DPPC or PyrPC acyl chain and the CM of the closest pyrene moiety in the same leaflet. Because the *sn*-2 hydrocarbon chain of PyrPC has been replaced by a fluorescent probe, only the order parameter for the *sn*-1 chain is displayed in the case of PyrPC. For numbering of carbons, see Figure 1.

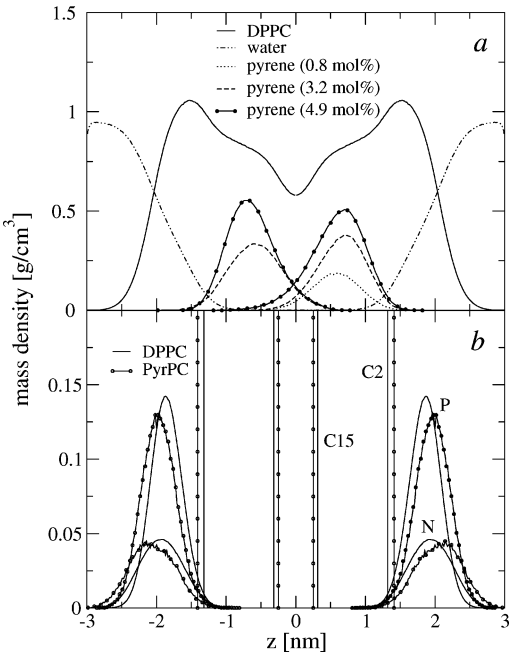

Figure 6. Mass density profiles for different system components across the membrane. (a) Profiles of the pyrene moieties, DPPCs, and water. The profiles for the position of pyrene for different concentrations correspond to the density of pyrene multiplied by a factor of 20. The profiles in the two leaflets are not identical because of limited sampling (and in the case of 0.8 mol % of PyrPC, there is actually only one PyrPC molecule in the system). The profiles of DPPC and water correspond to those in a pure DPPC system: corresponding profiles in membranes containing PyrPC are essentially identical to those shown here. (b) Profiles of P and N atoms in the headgroup. The vertical lines indicate the average positions of carbons 2 and 15 of the *sn*-1 acyl chains. Here, the profiles for PyrPC have been averaged over all three simulations that included varying amounts of PyrPC probes.

section IIIE (Conformations of Pyrene and Interdigitation) lead to a rapid decay of conformational disorder in the *sn*-2 chain, manifested as small order parameters in Figure 5.

D. Density Profiles. To study the preferred location of the pyrenyl group inside the lipid bilayer, we considered the mass density profiles of different molecular components along the bilayer normal. Because the bilayer's CM position may slightly fluctuate in time, we have determined the center of the bilayer in the *z*-direction separately for each frame of the simulation. Then the positions of all atoms were calculated with respect to the instantaneous CM location of the membrane. Given the bilayer symmetry, the mass density profiles were finally averaged over the two leaflets so that the position $z = 0$ corresponds to the center of the bilayer.

Mass density contributions from different molecular components of the system, as well as from a few particular atoms, are shown in Figure 6. Despite the relatively large size of the pyrene moiety, the density profile of DPPC was not observed to change (data not shown): the DPPC profiles with varying amounts of PyrPC were essentially similar and only the thickness of the membrane changed slightly. To quantify this, we defined the membrane thickness as the distance between the two points where the mass densities of water and lipids of each leaflet match. Our simulations indicated only a minor increase in membrane thickness for an increasing PyrPC concentration, the increase being about 0.03 nm. On the other hand, the conformations and locations of individual PyrPC molecules are clearly influenced by the attached fluorophore. PyrPC headgroups are less deeply integrated into the bilayer than the headgroups of native DPPC molecules, which can be seen by the displacements of headgroup phosphorus and nitrogen densities toward the membrane−water interface (Figure 6b). Equally evident are changes in the profiles of hydrocarbon chains, see Figure 6b: the average positions of carbons 2 and 15 of the *sn*-1 chains indicate that the PyrPC chains are more extended than the DPPC acyl chains. Both of the above observations are in line with the S_{CD} order parameter results and highlight the ordered nature of PyrPC and the preference of its headgroup for protrusions toward water.

The location of the pyrene moiety itself is rather well-defined. Figure 6a shows that it resides in the hydrocarbon chain region, though pyrene is not embedded at a fixed depth in the bilayer but can move within a broad range of transversal positions.

Using the quenching of fluorescence in POPC bilayers, Sassaroli et al.[15] determined the mean depth of pyrenyl CM in the bilayer to 1.1 nm from the membrane−water interface. Martins and Melo[9] have suggested that this value is underestimated by 0.3 nm because Sassaroli et al. considered phospholipid chains to be in random conformations, while in fluid bilayers of saturated lipids there is considerable ordering among lipid acyl chains. On the other hand, what neither of refs 9 or 15 accounted for is the fact that PyrPCs are more extended than DPPCs (see Figure 6): the length of PyrPC in the membrane normal direction is about 0.3−0.4 nm larger than that of DPPC (measured from C15 to N), and the headgroup of PyrPC is more deeply immersed into the water phase than the headgroup of DPPC. This effect seems to compensate for the effect of lipid chain ordering proposed in ref 9. Summarizing, the experiments of Sassaroli et al.[15] propose that the mean depth of pyrene moieties is about 1.1 nm from the membrane−water interface. For comparison, if we define the membrane−water interface as the mean position of glycerol carbon C13 (like it is illustrated in Figure 1 in ref 15), then the corresponding value found from

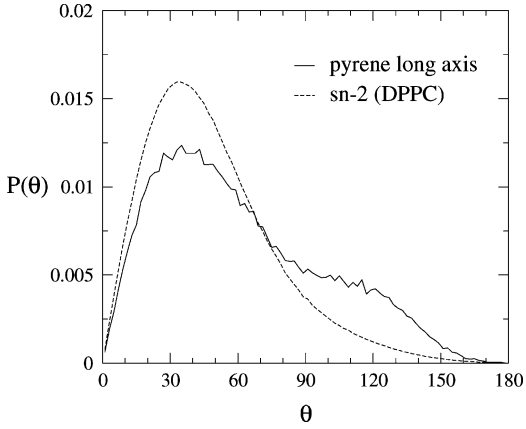

Figure 7. Probability distribution function $P(\theta)$ of pyrene long axis orientation. The θ is the angle between the bilayer normal pointing toward water from a given monolayer and the vector joining the pyrene carbons 15′ and 6′ (for numbering of atoms see Figure 1). For comparison, we also show a similar plot for the *sn*-2 chain of nonlabeled DPPCs. In this case, the vector is from carbon 16 to 11 in the chain (see Figure 1).

our MD simulations is 0.8 nm, in reasonably good agreement with the value given by Sassaroli et al.

Overall, these observations together with the results for $\langle A \rangle$ indicate that the addition of relatively small amounts of pyrene-labeled lipids into DPPC bilayers has only a weak effect on the global structural properties of the membrane. For considerably larger concentrations of PyrPC, the situation may obviously be different.

E. Conformations of Pyrene and Interdigitation. A more detailed picture of the manner by which the pyrene moiety is incorporated into the membrane structure is given by the orientational probability distribution $P(\theta)$, where θ is the angle between the bilayer normal pointing toward water from a given leaflet and the pyrene long axis vector from carbon 15′ to carbon 6′.

Figure 7 shows that the probability distribution of pyrene orientation is rather broad, with a global peak at around 40° and a smaller peak close to 120°. The tail at large θ is particularly interesting because it indicates that a substantial portion (about 30%) of fluorophore molecules are pointing toward the membrane−water interface, that is, for θ larger than 90°. These orientations require a kink in the acyl chain conformation. This conformation has been suggested for dipyrenylphosphatidylcholine probes.[35]

To relate the instantaneous orientation of the pyrenyl long axis with the depth of the pyrene group in the bilayer, we show in Figure 8 a plot of θ as a function of pyrene CM position along the bilayer normal. We find that close to the membrane−water interface, all orientations except for $\theta \approx 180°$ are possible, including those where $\theta > 90°$. In the vicinity of membrane center, however, the orientations with $\theta > 90°$ are forbidden. This results from the extended conformation of PyrPC in this situation and from the fact that for θ larger than 90°, the chain should be kinked. What is most remarkable, however, is the substantial amount of conformations where $\theta \approx 30-60°$ and the pyrene group interdigitates to the opposed monolayer. Interdigitation of the CM of pyrene extends deep into the other monolayer up to a distance of about 0.8 nm, and this is just a lower limit because the finite size of the pyrene group and its van der Waals radius should also be taken into account (see also Figure 6a for the overlap of mass density profiles of pyrenes in different leaflets). Given that this is almost a half of leaflet thickness, this implies that the pyrene probe is occasionally in

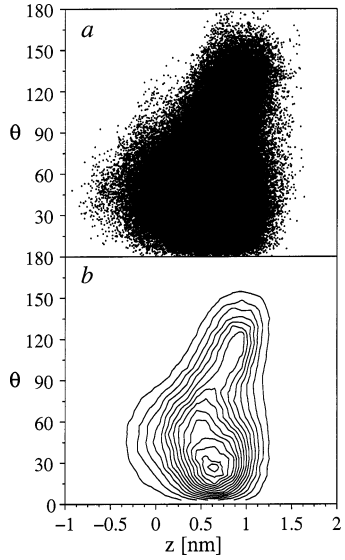

Figure 8. (a) Probability density plot of the pyrene long axis orientation with respect to membrane normal. The figure shows each realization of the three different simulations with varying amounts of pyrene. Here, *z* refers to the instantaneous CM position (its *z*-coordinate) of pyrene with respect to the CM position of the bilayer. Negative values of *z* correspond to interdigitation, where the pyrene resides in the opposite leaflet. (b) Same as in (a), but now shown as a contour plot to better illustrate the shape of the two-dimensional distribution.

contact with the lipid acyl chains as well as with the other pyrene probes in the opposite leaflet. These two scenarios are demonstrated in Figure 2.

The fraction of PyrPC molecules involved in interdigitation seems to slightly depend on PyrPC concentration. For the smallest PyrPC concentration (0.8 mol %) studied here, we found that in 3.6% of all the configurations, the CM of a PyrPC molecule was located in the opposing membrane leaflet. For larger molar concentrations of PyrPC, 3.2 mol % and 4.9 mol %, the corresponding fractions were found to be 4.0% and 5.7%, in respective order. Due to a small number of samples, however, these numbers should be considered as suggestive rather than conclusive.

The interdigitation of pyrene raises some concern about possible perturbations in the ordering of the acyl chains in the other leaflet. Hence, we analyzed configurations where the pyrene moiety was found to protrude into the other monolayer and calculated the order parameters of acyl chains in the opposite lipid leaflet. The order parameter profiles in Figure 9 show that the ordering of acyl chains in the vicinity of pyrene is enhanced due to interdigitation. However, the range of perturbations in this case is very small, of the order of 0.5 nm, and, hence, clearly smaller than for perturbations in the same leaflet (Figure 5). One is also tempted to conclude that the influence of pyrene on the *sn*-2 acyl chain would be stronger than the effect on the *sn*-1 chain, but the present data does not allow us to draw such a conclusion because of the rather large fluctuations associated with the case $R_{acyl} < 0.5$ nm (error estimate ± 0.04) For other curves in Figure 9, the errors are considerably smaller.

The facts that pyrene may protrude to the opposed leaflet and that this interdigitation can extend rather deep imply that pyrene labels can possibly form an excimer with the pyrenyl group in the opposite layer, see Figure 2. This possibility is in agreement with previous observations[9] concerning PyrPC probes in a DMPC bilayer. Obviously, this may complicate the interpretation of measured experimental data related to pyrene excimer formation. However, as interleaflet excimer formation

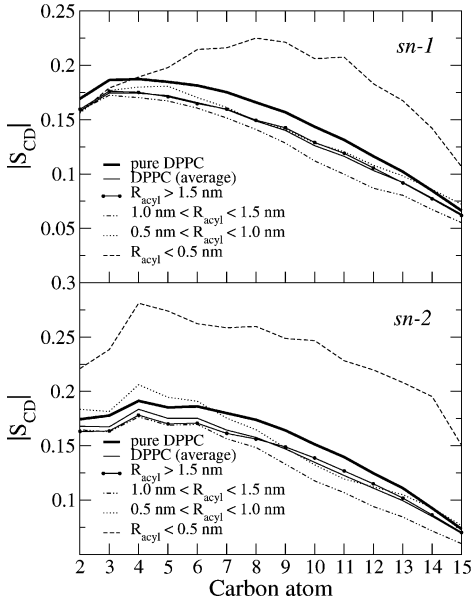

Figure 9. Order parameter $|S_{CD}|$ profiles for the *sn*-1 and *sn*-2 DPPC acyl chains that are near the pyrene label but in the opposite lipid monolayer. Here, R_{acyl} is the 3D distance between the CM of a DPPC acyl chain and the CM of the pyrene moiety (the two residing in different leaflets). The estimated error for curves with $R_{acyl} < 0.5$ nm is ± 0.04, and, hence, rather large because of the small number of events where the pyrene is in close contact with the acyl chain in the opposing leaflet. For curves associated with 0.5 nm $< R_{acyl} <$ 1.0 nm, the error is ± 0.015, and for $R_{acyl} > 1.0$ nm it is much smaller, about ± 0.005.

events may be rare events, and our study cannot quantify the corresponding rate, the significance of these events remains to be investigated.

IV. Concluding Remarks

Given that fluorescent probes are used extensively to explore a variety of membrane processes such as domain formation, lateral diffusion, and membrane fusion, it is somewhat surprising how little is known about the perturbations induced by the probes. The influence of diphenylhexatriene on a fluidlike saturated PC bilayer has been characterized,[8] but the effects of other commonly used probes such as pyrene have received much less attention. Free pyrene has been observed to decrease the average area per lipid in POPC bilayers.[19] Further studies of Langmuir monolayers comprised of PyrPCs have shown that the average area per molecule is slightly increased compared to pure DPPC monolayers. While there are no similar studies for the influence of pyrene labeling on lipid bilayers, a recent study by Koivusalo et al.[13] has shown that the length of the pyrene-labeled acyl chain affects the partitioning of the labeled lipid between gel and fluid domains: partitioning of a pyrene-labeled lipid shifted in favor of an ordered phase when the length of the labeled chain increased. While these recent observations support the idea that labeling inevitably perturbs membrane properties, the detailed nature of the influence of pyrene-labeling has remained an open issue, though.

In this work, we have performed MD simulations of fluorescently labeled model bilayers in the fluid phase to investigate the influence of pyrene-labeling on bilayer properties. We have found that the linkage of the pyrenyl group to the decanoyl chain of the phospholipid causes the fluorophore to reside deep in the hydrophobic core of the bilayer. PyrPC headgroups are slightly shifted toward the water environment, but the arrangement of the dipole vector is not affected in a significant manner. Due to the location of pyrene, most significant changes are observed in the hydrophobic part of the membrane where we find increased ordering and more tight packing of lipid acyl chains in the vicinity of the probe molecule. Nevertheless, the perturbations are of local nature because beyond a distance of about 1.0−1.5 nm from the pyrene (corresponding to about 2−3 molecular diameters and about 15 lipid molecules in the vicinity of the probe), the influence is almost negligible. This is confirmed by the observation that even for rather high concentrations of labeled molecules the general membrane properties (averaged over all lipids in the system) are not affected in a significant manner. This highlights the difficulties associated with experimental studies of probe-induced perturbations and also demonstrates how simulation studies can complement experiments in a highly useful manner. Interestingly, however, we have found that the perturbations induced by pyrene are not confined to the leaflet in which the labeled lipid resides. Instead, due to significant interdigitation, the pyrene moieties perturb lipids in the opposite leaflet, too. Consequently, our results support the idea that the formation of excited-state pyrene dimers (excimers) may take place for pyrenes in different leaflets.[9]

We found that the results for different PyrPC concentrations (0.8, 3.2, and 4.9 mol %) are largely identical. This might suggest that PyrPC-induced perturbations do not significantly depend on the probe concentration. However, this idea should be taken with some reservation. For increasing amounts of PyrPC, we found a slight increase in the interdigitation of pyrene into the opposed leaflet. Further, even though the simulations reported in this work have been very long on current standards (about 140 ns in each of the four cases studied), it is clear that the simulated time scale is short compared to times characteristic to the clustering of and collisions between different PyrPC molecules. Given this, and the fact that our simulations were started from an initial state where PyrPCs were not in close contact, we cannot exclude the possibility that collective effects through excimer formation and PyrPC clustering might enhance perturbations of membrane structure and dynamics at larger PyrPC concentrations. The role of such concerted events for membrane perturbations remains to be investigated.

Considering other bilayer systems, it is tempting to ask what happens if the bilayer of DPPCs is replaced by, say, a membrane comprised of other saturated PC lipids with longer hydrocarbon chains. Concerning the properties of pyrene probes, perhaps the most obvious change then is an increase in membrane thickness: because the headgroups of PyrPC probes are bound to the membrane−water interface, an increase in membrane thickness is expected to result in reduced interdigitation and, consequently, also reduced interleaflet excimer formation. The same scenario applies to highly ordered domains rich in cholesterol and sphingomyelin, that is, lipid rafts. Obviously, the interdigitation of pyrene-linked lipids depends on the interplay between the length of the pyrene-linked lipid moiety and the lipid content surrounding the probe.

Overall, the character of the changes observed in this work is very similar to perturbations induced by another commonly used fluorescent probe, free diphenylhexatriene.[8] It is likely that more substantial effects are induced by pyrene-labeled phospholipids in the gel phase, where the acyl chains are ordered and the bulky pyrene group is expected to significantly perturb the packing of acyl chains. Work is in progress to address this possibility.

Acknowledgment. Ole Mouritsen and Paavo Kinnunen are thanked for discussions. This work has, in part, been supported by the Academy of Finland through its Center of Excellence Program (J.R., I.V.), the Academy of Finland Grant Nos. 80246

(I.V.) and 54113 (M.K.), and by Emil Aaltonen Foundation (M.K.). J.M.H. is supported by Sigrid Juselius Foundation and Oskar Huttunen Foundation. We would also like to thank the Finnish IT Center for Science and the HorseShoe (DCSC) supercluster computing facility at the University of Southern Denmark for computer resources.

Abbreviations

DPPC	dipalmitoyl phosphatidyl choline
PyrPC	1-palmitoyl-2-(1-pyrenedecanoyl)-*sn*-glycero-3-phosphocholine
POPC	1-palmitoyl-2-oleoyl phosphatidyl choline
DMPC	dimyristoyl phosphatidyl choline
NMR	nuclear magnetic resonance
MD	molecular dynamics
CM	center of mass

References and Notes

(1) Mouritsen, O. G. *As a Matter of Fat-The Emerging Science of Lipidomics*; Springer-Verlag: Heidelberg, Germany, 2005.

(2) Gennis, R. B. *Biomembranes: Molecular Structure and Function*; Springer-Verlag: New York, 1989.

(3) *Lipid Bilayers: Structure and Interactions*; Katsaras, J., Gutberlet, T., Eds.; Springer-Verlag: Berlin, Germany, 2001.

(4) Pownall, H. J.; Smith, L. C. *Chem. Phys. Lipids* **1989**, *191*, 191−211.

(5) Somerharju, P. *Chem. Phys. Lipids* **2002**, *116*, 57−74.

(6) Maier, O.; Oberle, V.; Hoekstra, D. *Chem. Phys. Lipids* **2002**, *116*, 3−18.

(7) Repáková, J.; Èapková, P.; Holopainen, J. M.; Vattulainen, I. *J. Phys. Chem. B* **2004**, *108*, 13438−13448.

(8) Repáková, J.; Holopainen, J. M.; Morrow, M. R.; McDonald, M. C.; Èapková, P.; Vattulainen, I. *Biophys. J.* **2005**, *88*, 3398−3410.

(9) Martins, J.; Melo, E. *Biophys. J.* **2001**, *80*, 832−840.

(10) Blumenthal, R.; Gallo, S. A.; Viard, M.; Raviv, Y.; Puri, A. *Chem. Phys. Lipids* **2002**, *116*, 39−55.

(11) Hresko, R. C.; Sugar, I. P.; Barenholz, Y.; Thompson, T. E. *Biochemistry* **1986**, *25*, 3813−3823.

(12) Galla, H.-J.; Sackmann, E. *J. Am. Chem. Soc.* **1975**, *97*, 4114−4120.

(13) Koivusalo, M.; Alvesalo, J.; Virtanen, J. A.; Somerharju, P. *Biophys. J.* **2004**, *86*, 923−935.

(14) Holopainen, J. M.; Metso, A. J.; Mattila, J. P.; Jutila, A.; Kinnunen, P. K. J. *Biophys. J.* **2004**, *86*, 1510−1520.

(15) Sassaroli, M.; Ruonala, M.; Virtanen, J.; Vauhkonen, M.; Somerharju, P. *Biochemistry* **1995**, *34*, 8843−8851.

(16) Saiz, L.; Klein, M. L. *Acc. Chem. Res.* **2002**, *35*, 482−489.

(17) Scott, H. L. *Curr. Opin. Struct. Biol.* **2002**, *12*, 495−502.

(18) Vattulainen, I.; Karttunen, M. In *Computational Nanotechnology*; Rieth, M., Schommers, W., Eds.; American Scientific Press: New York, 2005.

(19) Hoff, B.; Strandberg, E.; Ulrich, A. S.; Tieleman, D. P.; Posten, C. *Biophys. J.* **2005**, *88*, 1818−1827.

(20) Berger, O.; Edholm, O.; Jahnig, F. *Biophys. J.* **1997**, *72*, 2002−2013.

(21) Chiu, S. W.; Clark, M.; Balaji, V.; Subramaniam, S.; Scott, H. L.; Jakobsson, E. *Biophys. J.* **1995**, *69*, 1230−1245.

(22) Berendsen, H. J. C.; Postma, J. P. M.; van Gunsteren, W. F.; Hermans, J. In *Intermolecular Forces*; Pullman, B., Ed.; Reidel: Dordrecht, 1981; pp 331−342.

(23) Patra, M.; Karttunen, M.; Hyvönen, M. T.; Falck, E.; Lindqvist, P.; Vattulainen, I. *Biophys. J.* **2003**, *84*, 3636−3645.

(24) Patra, M.; Karttunen, M.; Hyvönen, M. T.; Falck, E.; Vattulainen, I. *J. Phys. Chem. B* **2004**, *108*, 4485−4494.

(25) Lindahl, E.; Hess, B.; van der Spoel, D. *J. Mol. Model.* **2001**, *7*, 306−317.

(26) Berendsen, H. J. C.; Postma, J. P. M.; van Gunsteren, W. F.; DiNola, A.; Haak, J. R. *J. Chem. Phys.* **1984**, *81*, 3684−3690.

(27) Hess, B.; Bekker, H.; Berendsen, H. J. C.; Fraaije, J. G. E. M. *J. Comput. Chem.* **1997**, *18*, 1463−1472.

(28) Janiak, M. J.; Small, D. M.; Shipley, G. G. *Biochemistry* **1976**, *15*, 4575−4580.

(29) Nagle, J. F.; Tristram-Nagle, S. *Biochim. Biophys. Acta* **2000**, *1469*, 159−195.

(30) Somerharju, P. J.; Virtanen, J. A.; Eklund, K. K.; Vainio, P.; Kinnunen, P. K. J. *Biochemistry* **1985**, *24*, 2773−2781.

(31) Kaznessis, Y. N.; Kim, S.; Larson, R. G. *Biophys. J.* **2002**, *82*, 1731−1742.

(32) Murzyn, K.; Róg, T.; Jezierski, G.; Takaoka, Y.; Pasenkiewicz-Gierula, M. *Biophys. J.* **2001**, *81*, 170−183.

(33) Petrache, H. I.; Dodd, S. W.; Brown, M. F. *Biophys. J.* **2000**, *79*, 3172−3192.

(34) Metso, A. J.; Jutila, A.; Mattila, J.-P.; Holopainen, J. M.; Kinnunen, P. K. J. *J. Phys. Chem. B* **2003**, *107*, 1251−1257.

(35) Holopainen, J. M.; Lehtonen, J. Y. A.; Kinnunen, P. K. J. *Biophys. J.* **1999**, *76*, 2111−2120.